TU Delft

Delft University of Technology

Size Effect in the Compression of 3D Polymerized Micro-Structures

Li, Jiayu; Accardo, Angelo; Liu, Shutian

DOI
10.1115/1.4063028

Publication date
2024

Document Version
Final published version

Published in
Journal of Applied Mechanics, Transactions ASME

Citation (APA)
Li, J., Accardo, A., & Liu, S. (2024). Size Effect in the Compression of 3D Polymerized Micro-Structures. *Journal of Applied Mechanics, Transactions ASME*, *91*(1), Article 011002. https://doi.org/10.1115/1.4063028

Important note
To cite this publication, please use the final published version (if applicable).
Please check the document version above.

Copyright
Other than for strictly personal use, it is not permitted to download, forward or distribute the text or part of it, without the consent of the author(s) and/or copyright holder(s), unless the work is under an open content license such as Creative Commons.

Takedown policy
Please contact us and provide details if you believe this document breaches copyrights.
We will remove access to the work immediately and investigate your claim.

This work is downloaded from Delft University of Technology.
For technical reasons the number of authors shown on this cover page is limited to a maximum of 10.

Green Open Access added to TU Delft Institutional Repository

'You share, we take care!' - Taverne project

https://www.openaccess.nl/en/you-share-we-take-care

Otherwise as indicated in the copyright section: the publisher is the copyright holder of this work and the author uses the Dutch legislation to make this work public.

Check for updates

ASME Journal of Applied Mechanics
Online journal at:
https://asmedigitalcollection.asme.org/appliedmechanics

Jiayu Li
State Key Laboratory of Structural Analysis, Optimization and CAE Software for Industrial Equipment,
Dalian University of Technology,
Dalian, Liaoning 116024, China
e-mail: li_jy@mail.dlut.edu.cn

Angelo Accardo
Department of Precision and Microsystems Engineering,
Faculty of Mechanical Maritime and Materials Engineering,
Delft University of Technology (TU Delft),
Mekelweg 2, Delft 2628 CD, The Netherlands
e-mail: a.accardo@tudelft.nl

Shutian Liu[1]
State Key Laboratory of Structural Analysis, Optimization and CAE Software for Industrial Equipment,
Dalian University of Technology,
Dalian, Liaoning 116024, China
e-mail: stliu@dlut.edu.cn

Size Effect in the Compression of 3D Polymerized Micro-Structures

Micro/nanoscale additive manufacturing provides a powerful tool for advanced materials and structures with complex and precise features. For instance, the feature resolution of two-photon polymerization (2PP) can reach 200 nm. At this scale, materials properties can change, and the influence of the size effect cannot be ignored. Therefore, it is necessary to assess changes in the material mechanical properties considering size effects. In this work, several micrometric polymeric specimens are printed via 2PP, and their mechanical properties are assessed using compression tests. Detailed printing and testing procedures and the effects of parameter settings are provided. The experimental results show that the changes in the microstructures' size have a direct effect on Young's modulus. In particular, a large surface-volume ratio results in a higher Young's modulus. In other words, the smaller the structure size, the higher the stiffness. The reported findings play a significant role in the development of fabrication strategies for polymeric microstructures where high stiffness accuracy is fundamental. [DOI: 10.1115/1.4063028]

Keywords: size effect, micro/nanoscale additive manufacturing, two-photon polymerization resin, Young's modulus, mechanical properties of materials

1 Introduction

The rapid development of additive manufacturing (AM) has significantly impacted the manufacturing industry, greatly promoting the development of lightweight micro- and nano-structures, reinforced structural materials, biomedical devices, and micrometer-length scale sensors and detectors [1]. For example, AM has enabled many efficient material structures, such as ultralight metallic micro-lattices [2], hierarchical architected metamaterials [3], 3D nano-scaffolds for bone implants [4], 3D polymer and hydrogel microenvironments engineered for cell culture applications [5], and chiral metamaterials for molding the polarization and direction of elastic waves [6]. In AM techniques, two-photon polymerization (2PP) is a powerful and useful manufacturing tool that enables photosensitive resin printing with a minimum feature size of 200 nm by initiating polymerization in a very small volume region by absorbing simultaneously two infrared photons. Based on 2PP technology, Maggi et al. [4] proposed to cultivate bone cells with three-dimensional nano-scaffolds with variable stiffness; Bauer et al. [7] obtained a high-strength glass-carbon nanocrystalline lattice through pyrolysis, second in strength only to diamond; Nguyen and Narayan [8] reviewed the application of 2PP in the field of bioengineering; Qu et al. [9] realized negative pressure metamaterial under quasi-static conditions; Kotz et al. [10] printed three-dimensional fused silica microstructures with high thermal, chemical, and mechanical stability, and surface roughness of only 6 nm. Sharaf et al. [11] fabricated 3D microstructures to foster a ramified resting phenotype in primary microglia, which paved the way for studying these cells in both healthy and diseased conditions.

For these advanced materials and structures printed by AM, the corresponding properties analysis also faces new requirements and challenges. Almost all materials exhibit different properties when scaled down to nanometer or micrometer sizes [12,13], such as stiffness changes [14–17], negative effective compressibility [9], lower refractive index [18], smaller is more ductile or deformable [19], and control of photoluminescence in elastic photonic crystals [20]. In a structural stiffness and strength study, Albiez and Schwaiger [14] conducted compression tests on glass-carbon nanorods and observed that smaller structure size results in higher strength, which may be due to the fact that small structures feature fewer defects and lower defect density. Sun et al. [16] reported the uniaxial compression test results of rectangular titanium microcolumns under loading. In the presence of 300 nm microcolumns, the strength is decreased to 16% of the theoretical strength of titanium. Gu et al. [17] studied the size-dependent deformation of nanocrystalline Pt nanopillars and found that the smaller the size, the lower the strength. The work also pointed out that size-dependent behavior is associated with distinct deformation mechanisms operating in the interior versus surface grains. Therefore, it is possible to conclude that basic research on mechanical properties is essential for additively manufactured micro/nanoscale structures, and the influence of size effect on stiffness cannot be ignored.

Currently, most of the research on 2PP focuses on innovative structure design, while research on its mechanical properties is also in progress. Dimitriadis et al. [21] conducted atomic force microscope nanoindentation experiments to measure soft materials' elastic moduli at microscopic scales. Lemma et al. [22] obtained Young's modulus, Poisson's ratio, material density, and viscosity through static and dynamic analyses (micro-bending of pillar-like

[1]Corresponding author.

Contributed by the Applied Mechanics Division of ASME for publication in the Journal of Applied Mechanics. Manuscript received April 30, 2023; final manuscript received July 17, 2023; published online August 25, 2023. Assoc. Editor: Pradeep Sharma.

 Copyright © 2023 by ASME

Downloaded from http://asmedigitalcollection.asme.org/appliedmechanics/article-pdf/91/1/011002/7036641/jam_91_1_011002.pdf by Bibliotheek Tu Delft user on 18 September 2023

structures and picometer-sensitive laser Doppler vibrometry of drum-like structures). The experiment also proved that the laser exposure power is a crucial parameter to define the stiffness of the realized structures, with hyper-elasticity observable for high-power polymerization, which can affect the structure's stiffness. Liu et al. [23] examined the mechanical strength of beam and foam structures during the development and drying processes and pointed out that the substantial shrinkage in IP-Dip (~5–10%) causes large shear stresses and associated plastic deformation, particularly near constrained boundaries and locations with sharp density transitions. Concerning the study of size effect, Montemayor and Greer [24] presented the fabrication and mechanical properties of three-dimensional hollow gold nanolattices whose compressive responses demonstrate that strength and stiffness vary as a function of geometry and tube wall thickness. Albiez and Schwaiger [14] compressed glassy carbon nanotubes of different sizes and found that small nanotubes exhibit elastoplastic deformation before failure. In addition, the strength value of the smaller nanorods was higher, and it was suggested that this might be related to the smaller defects and the lower defect concentration in the material. However, the measured mechanical properties were not the ones of the polymer itself but those of the polymer after pyrolysis. To the best of our knowledge, there is no reported size effect study on 2PP materials.

In this work, a two-photon polymerization laser printer was employed to print polymeric structures, and the mechanical properties of the IP-Dip material were obtained via compression tests. We reported that the effect of size is significant, particularly the impact of cross-sectional area and height on Young's modulus, which should be considered when printing polymeric materials at the micro-scale with high mechanical accuracy requirements.

2 Experimental Section

2.1 Two-Photon Polymerization Setup

2.1.1 Design of the Structures. All the structures were designed with SOLIDWORKS 2019 and imported into NANOSCRIBE Describe software, which converts STL files into Nanoscribe's General Writing Language (GWL). The GWL file was provided to the NanoWrite program that controls the 2PP system. The structures were several series of rectangular pillars with different heights and cross-sectional areas for size effect analysis. The specific geometries are reported in Sec. 3.

2.1.2 Material and Substrate Preparation. The microstructures were made of IP-Dip, a liquid negative-tone 2PP resin specifically designed for the dip in laser lithography (DiLL) technology to print the finest possible features. The structures were manufactured onto fused silica substrates featuring a size of $25 \times 25 \times 0.7\ \text{mm}^3$. The substrate was cleaned with acetone, isopropyl alcohol, and dried with an air gun. Then the substrate underwent an oxygen plasma process (Diener Femto plasma etcher) at a power of 80 W for 5 min, O_2 flow at 5 sccm, and pressure of 0.1 bar, which cleans and activates to enable higher adhesion of the printed structure to the substrate.

2.1.3 Two-Photon Polymerization Setup Configuration. The 2PP system (Nanoscribe Photonic Professional GT+) was employed to manufacture the structures. Short infrared laser pulses at 780 nm wavelength were tightly focused into a photopolymerizable resin. A configuration was used where galvanic mirrors scan the laser beam laterally, and the vertical movement was carried out with piezo actuation of the stage. We employed DiLL configuration in which the objective (63×, NA 1.4) was dipped in the photoresist. Laser power and scan speed were 40 mW and 10,000 μm/s, respectively. The parameters of slicing (distance between adjacent layers) and hatching (lateral distance between adjacent lines) were set to 100 nm. After printing, the polymerized structures on the substrate were carefully placed horizontally in a borosilicate petri dish containing propylene glycol monomethyl ether acetate (PGMEA) for 25 min to dissolve the unpolymerized resin. The structures were then soaked in isopropanol for 5 min to rinse off excess PGMEA and finally dried with an air gun.

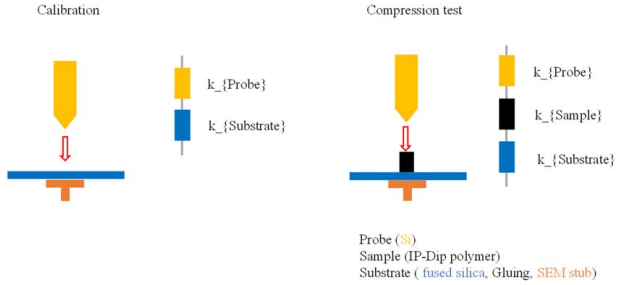

Fig. 1 Schematic diagram of compression test and calibration

2.2 Scanning Electron Microscopy Characterization. Scanning electron microscopy (SEM) was employed to characterize the structure morphologically and to monitor the alignment between the structure and the tip of the mechanical compression testing tool (see the following subsections for details). A JEOL JFC-1300 auto-fine sputter coater at 10 mA for 100 s (pressure 0.5 mbar) was used, with samples at 25 mm distance from the source leading to a gold layer of 10–30 nm in order to reduce charging effects on the polymeric materials. A JEOL JSM-6010LA SEM was used in a high-vacuum with an accelerating voltage of 5 kV.

A series of cubes were printed to check whether the fabricated structure was consistent with the nominal designed features. The results (Supplementary Fig. S1) show that the error between the printed structure and the design is less than 1%. In this way, the design dimensions are used for subsequent mechanical analysis and calculations.

2.3 Mechanical Characterization. The Femtotools nanomechanical testing system FT-NMT03 was employed to extract Young's modulus of manufactured structures. A uniaxial compression test was performed by applying a load onto the structures and measuring the deformation using a position encoder. A Si probe, capable of measuring forces from $-200{,}000\ \mu$N to $+200{,}000\ \mu$N, with a $50\ \mu\text{m} \times 50\ \mu\text{m}$ flat punch pin, was employed. The compression test was based on a given displacement, where the displacement measured contains the system and the sample (Fig. 1). The system stiffness includes SEM stub (screwed on tight), superglue, substrate (fused silica), and probe, which can be calibrated by conducting compression tests directly on the stub/glue/substrate. The compression displacement of the calibration was set to 3% of the structure height, while 10–70% of the force/displacement curve was considered for the analysis (Supplementary Fig. S2). Since the material is viscoelastic and the stiffness is time-dependent, the compression time for samples was set to the same 1 s. The compression displacement was set to 3% of the height of the structures within the linear elastic range, and the compression speed was proportional to the height of the compression displacement. Therefore, 11 groups of system stiffness with the compression displacement increasing from 0.36 μm to 1.56 μm listed in Table 1, should be set accordingly before the structural test.

3 Results and Discussion

In order to explore the size effect of the micro-scale structures printed by IP-Dip material used in a high-precision two-photon polymer printer, four sets of pillars with rectangular cross sections were printed, and compression tests were conducted on them. The

Downloaded from http://asmedigitalcollection.asme.org/appliedmechanics/article-pdf/91/1/011002/7036641/jam_91_1_011002.pdf by Bibliotheek Tu Delft user on 18 September 2023

Table 1 System stiffness at different compression displacements (compression onto the substrate directly)

Displacement (μm)	0.36	0.48	0.6	0.72	0.84	0.96	1.08	1.2	1.32	1.44	1.56
Stiffness (N/m)	26,223	26,782	27,022	27,127	27,515	27,598	27,678	27,772	27,723	27,861	27,901

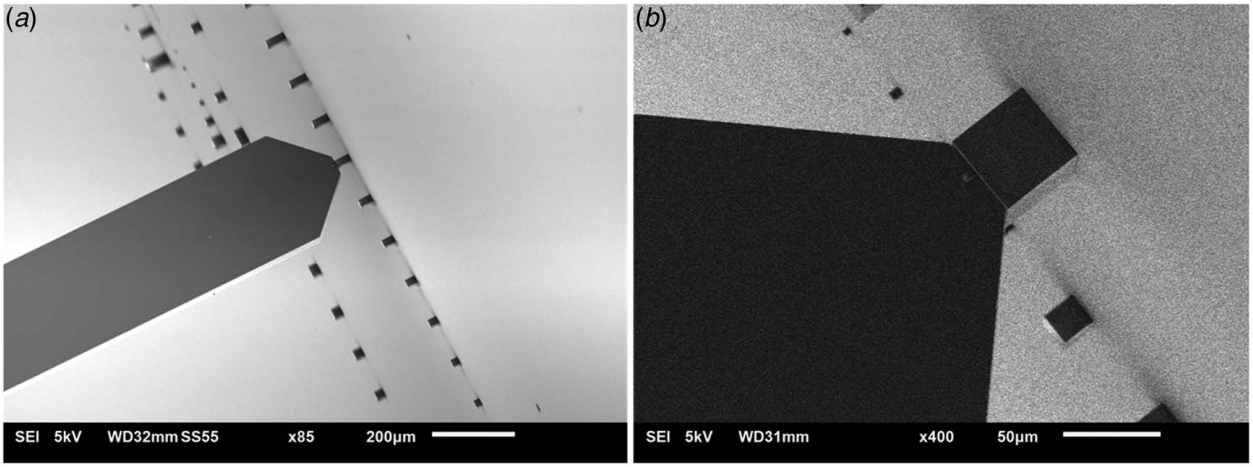

Fig. 2 SEM micrographs of compression test: (*a*) a group of pillars of different heights is printed and the schematic diagram of compression test is carried out and (*b*) 50 μm × 50 μm × 50 μm IP-Dip cube under compression

same experiment was repeated three times to obtain a mean value and standard deviation.

Figure 2(*a*) shows the schematic diagram of tested pillars of different heights. The cross-sectional size of the probe is 50 μm × 50 μm. In extreme case, Fig. 2(*b*) shows the 50 μm × 50 μm × 50 μm IP-Dip cube under compression. Obviously, the probe should be larger than the cross section of structures and the probe center should be located in the center of the central axis.

3.1 Characterization of Young's Modulus. The strain of the structure under compression is expressed as

$$\varepsilon = \frac{\Delta l}{l} = \frac{\sigma}{E} = \frac{F}{AE} \tag{1}$$

$$E^* = \frac{Fl}{A\Delta l} = \frac{F}{\Delta l} \cdot \frac{H}{A} = k \cdot \frac{H}{A} \tag{2}$$

where H is the height, A is the area, k is the structural stiffness measured by compression from the slope of the curves within the linear elastic region, and E^* is Young's modulus of the structure measured by compression experiment.

Due to the presence of a gold layer, the measured structure's Young's modulus is not the Young's modulus of the polymer and needs to be further calculated according to the measured results. Considering the error of the gold sputtered, we assume that the structure to be tested consists of two parts. As shown in Fig. 3, the outer surface is gold sputtered about 20 nm before compression,

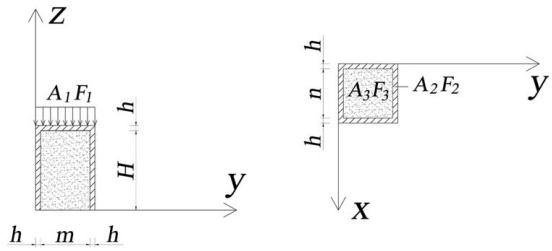

Fig. 3 Schematic of a pillar with gold-plated layer

while the middle is printed polymer. H is the thickness of the polymer; h is the thickness of gold; E_1, A_1, and F_1 are the stiffness, area, and force on the upper layer of the measured structure; E_2, A_2, and F_2 are the stiffness, area, and force on the side gold surface. E_3, A_3, and F_3 are the polymer's stiffness, area, and force, where $E_1 = E_2$, $A_1 = A_2 + A_3$, $F_1 = F_2 + F_3$, and m and n are the two sides of the rectangular section of the polymer. Therefore, Δl consists of two parts

$$\Delta l = \Delta l_1 + \Delta l_2 \tag{3}$$

Substituting from Eq. (1), we obtain the following equation:

$$\Delta l_1 = \frac{F_1 h}{E_1 A_1} \tag{4}$$

$$\Delta l_2 = \Delta l_3 = \frac{F_2 h}{E_2 A_2} = \frac{F_3 h}{E_3 A_3} \tag{5}$$

From this equation, we see that

$$F_2 + F_3 = \frac{\Delta l_2 E_2 A_2}{H} + \frac{\Delta l_2 E_3 A_3}{H} = F_1 \tag{6}$$

Therefore, Δl_2 can be obtained directly from Eq. (6).

$$\Delta l_2 = \frac{F_1 H}{E_2 A_2 + E_3 A_3} \tag{7}$$

Equation (3) now becomes

$$\Delta l = \frac{F_1 h}{E_1 A_1} + \frac{F_1 H}{E_2 A_2 + E_3 A_3} \tag{8}$$

Thus, the equation for E^* becomes

$$E^* = \frac{H + h}{\left(\frac{h}{E_1 A_1} + \frac{H}{E_2 A_2 + E_3 A_3}\right) A_1} \tag{9}$$

From Eq. (9), Young's modulus of polymer E_3 is finally retrieved, where h is determined by the sputtering setting and

Downloaded from http://asmedigitalcollection.asme.org/appliedmechanics/article-pdf/91/1/011002/7036641/jam_91_1_011002.pdf by Bibliotheek Tu Delft user on 18 September 2023

Table 2 Young's modulus of pillars with the same height and different cross-sectional areas

a (μm)	10	12	14	16	18	20	22
H (μm)	12	12	12	12	12	12	12
E^* (GPa)	2.24	2.05	1.80	1.48	1.25	1.19	1.18
E_3 (GPa)	1.62	1.53	1.36	1.09	0.91	0.88	0.89

Note: a is the pillar's side length, H is the pillar's height, E^* is Young's modulus of the structure, and E_3 is Young's modulus of the polymer.

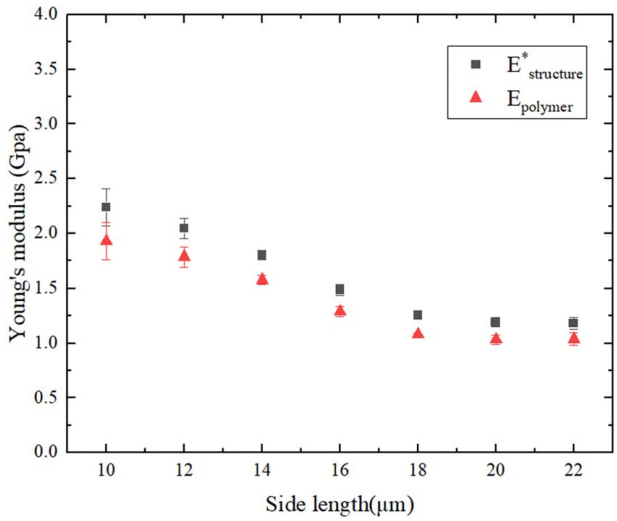

Fig. 4 Young's modulus of pillars with the same height and different cross-sectional areas

$E_1 = E_2 = 79$ GPa.

$$E_3 = \frac{HA_1}{\left(\frac{H+h}{E^*} - \frac{h}{E_1}\right)A_3} - \frac{E_2A_2}{A_3} \tag{10}$$

3.2 Influence of Cross-Sectional Area on Young's Modulus. The influence of cross-sectional area is reported in Table 2, where a is the side length of the square cross section and H is the height of the structure, E^* is Young's modulus of the structure, and E_3 is Young's modulus of the polymer. The side length of the square section is increased from 10 μm to 22 μm while the height is unchanged at 12 μm. Corresponding Young's modulus curves (Fig. 4) are obtained according to Eqs. (2) and (10), and the horizontal axis represents specimens of different side lengths. Compression displacement and speed are the same here. It can be seen that with the increase of side length, Young's modulus gradually converges to 0.88 GPa flat line, which we consider as the bulk Young's modulus. Therefore, the experiment shows that as the cross-sectional area decreases, the stiffness increases.

3.3 Influence of Height on Young's Modulus. In Table 3, the height of the pillars increases from 12 μm to 52 μm while the cross section remained set to 20 μm × 20 μm. As shown in Fig. 5, Young's modulus gradually increases with height. At the same time, for the height of 12 μm, the measured Young's modulus is the same as that in Table 2, which proves that the experimental data are accurate and reliable. It should be noted that the test speed is enlarged proportionately to the structural height to avoid stress relaxation, as the polymer is a viscoelastic material. Therefore, different probe speeds are set for pillars of different heights to ensure the same compression time, and the corresponding system stiffness should be set in advance.

Through the above experiments, the factors that cause stiffness change are the height and the side length of the cross section. Thus, we need to explore their influence on Young's modulus. In Table 4, the ratio of height-to-side length is kept equal. For the pillar with a height of 40 μm, the measured Young's modulus is the same as that in Table 3. It is still concluded that Young's modulus increased with the height increased. It could be seen that other influencing factors led to the inconsistency of the conclusion, such as slicing distance (SD), hatching distance, and test speed.

The SD is the thickness of each layer in the vertical direction of all structures, remained set to 100 nm. During the mechanical characterization, the compression time is the same, while the compression speed varies proportionally to the height. Therefore, the influence of SD should be considered since heights are different. A series of pillars with a height of 10 μm and a cross section of 10 μm × 10 μm are printed with SD of 0.1 μm, 0.2 μm, and 0.3 μm, respectively. The corresponding stiffness is shown in Table 5. The smaller SD is, the greater the stiffness is. A small slicing distance in bulk can lead to enhanced photopolymerization of the resist. Therefore, the test speed and SD are the main reason for the increase in stiffness in Figs. 5 and 6 and should be maintained in equal proportion. Lemma et al. [22], Sharaf et al. [25], and van Altena and Accardo [26] also reported that Young's moduli of stiff and soft materials can be tuned according to fabrication and post-treatment parameters.

3.4 Influence of Surface-to-Volume Ratio on Young's Modulus. At the same test speed, the height and cross-sectional area are the same, but the cross-sectional shape, namely the perimeter, is changed. In Table 6, m and n are the lengths of the two sides of the rectangular section, L is the circumference of the section, A is the area of the section, H is the pillar's height, and E^* is Young's modulus of the pillar. In Fig. 7, Young's modulus increases slightly as the perimeter continues to increase.

In Fig. 7, it is assumed that all pillars' heights and cross-sectional areas are the same, while the lateral surface area changes. This time, the height is not affected by SD and test speed. In order to describe the relationship between height and area more accurately, let t be the surface thickness of polymer, and Q be the ratio of the surface volume to the polymer volume, which is the surface-volume ratio times the thickness of the surface layer, then

$$Q = \frac{(S_{\text{upper,lower}} + S_{\text{lateral}})^* t}{\text{volume}} = \frac{2At + 2^*(m+n)^*H^*t}{A^*H} = \frac{2t}{H} + \frac{2Lt}{A} \tag{11}$$

Table 3 Young's modulus of pillars with the same cross-sectional area and different heights

a (μm)	20	20	20	20	20	20	20	20	20	20	20
H (μm)	12	16	20	24	28	32	36	40	44	48	52
E^* (GPa)	1.28	1.74	2.08	2.53	2.63	2.99	3.17	3.41	3.57	3.58	3.69
E_3 (GPa)	0.97	1.42	1.77	2.22	2.32	2.69	2.86	3.11	3.27	3.28	3.39

Note: a is the pillar's side length, H is the pillar's height, E^* is Young's modulus of the structure, and E_3 is Young's modulus of the polymer.

Downloaded from http://asmedigitalcollection.asme.org/appliedmechanics/article-pdf/91/1/011002/7036641/jam_91_1_011002.pdf by Bibliotheek Tu Delft user on 18 September 2023

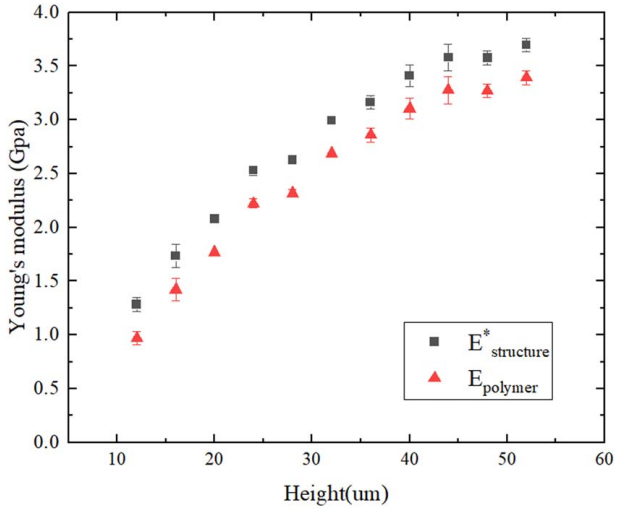

Fig. 5 Young's modulus of pillars with the same cross-sectional area and different heights

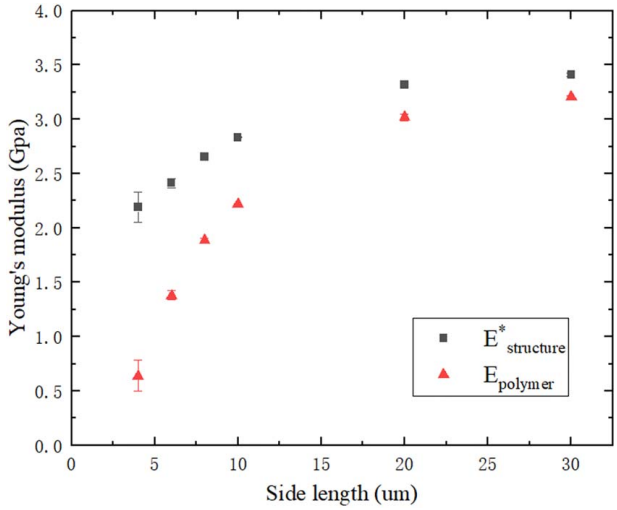

Fig. 6 Young's modulus of pillars with the same height-to-side length ratio

Table 4 Young's modulus of pillars with the same height-to-side length ratio

a (μm)	4	6	8	10	20	30
H (μm)	8	12	16	20	40	60
E^* (GPa)	2.19	2.41	2.65	2.83	3.33	3.41
E_3 (GPa)	0.64	1.38	1.89	2.22	3.02	3.21

Note: a is the pillar's side length, H is the pillar's height, E^* is Young's modulus of the structure, and E_3 is Young's modulus of the polymer.

Table 5 Young's modulus of pillars with different layer thicknesses

SD (μm)	0.1	0.2	0.3
E^* (GPa)	2.23	1.99	1.26

Note: SD is the slicing distance, and E^* is Young's modulus of the structure.

when the section is a square with sides of length a: $m=n=a$, $L=4a$, and $A=a^2$

$$Q=\frac{2t}{H}+\frac{4t}{a} \tag{12}$$

As discussed in Sec. 3.3, the change of H is also affected by the speed and SD, so this section only discusses the results of constant H. In Table 6, when A and H are constant, the increase of L leads to the increase of Q, and E_3 tends to increase. In Table 2, when H is constant, a decreases and Q increases accordingly, leading to an increase in E_3. The specific data are reported in the next section.

3.5 Mechanism Analysis. This paper demonstrates that the experimental results are correlated to the influence of surface effects. Therefore, the mechanical properties of the material's surface are different from those of the bulk material [27]. In additive manufacturing processes, the structure is built through the successive deposition, photopolymerization, or sintering of materials at the micro- or nanometer scale. As the thickness of the photopolymerized layers is 100 nm, several layers of material on the surface were assumed to have different material properties compared to the bulk.

Table 6 Young's modulus of pillars with the same height and cross-sectional area but different perimeters

H (μm)	24	24	24	24	24	24
m (μm)	24	22	20	18	16	14
n (μm)	24	26.18	28.8	32	36	41.14
Perimeter (μm)	96	96.36	97.6	100	104	110.29
Area (μm^2)	576	576	576	576	576	576
E^* (GPa)	3.02	3.06	3.21	3.23	3.29	3.55
E_3 (GPa)	2.55	2.59	2.74	2.75	2.80	3.04

Note: H is the pillar's height, m and n are the lengths of the two sides of the rectangular section, Perimeter is the circumference of the section, A is the area of the section, E^* is Young's modulus of the structure, and E_3 is Young's modulus of the polymer.

In order to analyze the reason for the influence of cross-sectional area on Young's modulus, the surface thickness t is set to 200 nm and 400 nm, respectively. The characterization of Young's modulus in Sec. 3.1 is used. The Young's modulus of the surface layer $E_{surface}$ is solved by using the equivalent Eq. (9), where E^* is the $E_{polymer}$ of the corresponding result in Table 2, and E_3 is the bulk material set to 0.88 GPa. As shown in Tables 7 and 8, as

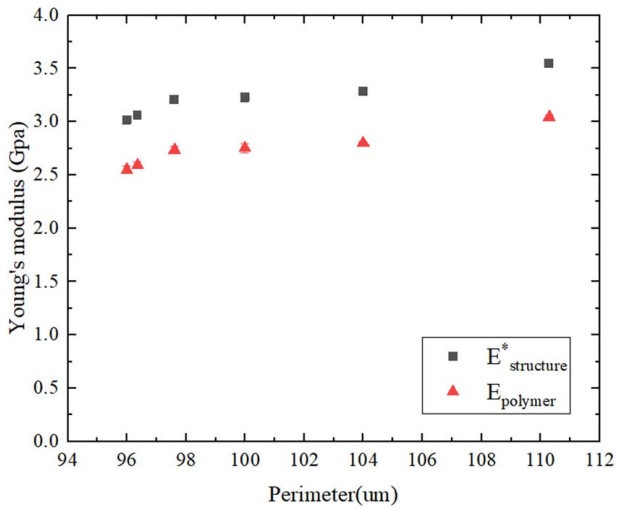

Fig. 7 Young's modulus of pillars with the same height and cross-sectional area but different perimeters

Downloaded from http://asmedigitalcollection.asme.org/appliedmechanics/article-pdf/91/1/011002/7036641/jam_91_1_011002.pdf by Bibliotheek Tu Delft user on 18 September 2023

Table 7 Young's modulus of the surface layer with a surface thickness of 0.2 μm

s (μm)	H (μm)	t (μm)	Q	$E_{polymer}$ (GPa)	$E_{surface}$ (GPa)
22	12	0.2	5.30%	0.89	1.19
20	12	0.2	5.67%	0.88	0.82
18	12	0.2	6.11%	0.9	1.28
16	12	0.2	6.67%	1.09	4.84
14	12	0.2	7.38%	1.36	8.98
12	12	0.2	8.33%	1.53	10.5
10	12	0.2	9.67%	1.62	10.04

Note: s is the polymer's side length, H is the polymer's height, t is the surface thickness, Q is the ratio of the surface volume to the polymer volume, $E_{polymer}$ is Young's modulus of the polymer, and $E_{surface}$ is Young's modulus of the surface layer.

Table 8 Young's modulus of the surface layer with a surface thickness of 0.4 μm

s (μm)	H (μm)	t (μm)	Q	$E_{polymer}$ (GPa)	$E_{surface}$ (GPa)
22	12	0.4	10.61%	0.89	1.03
20	12	0.4	11.33%	0.88	0.85
18	12	0.4	12.22%	0.9	1.08
16	12	0.4	13.33%	1.09	2.80
14	12	0.4	14.76%	1.36	4.86
12	12	0.4	16.67%	1.53	5.65
10	12	0.4	19.33%	1.62	5.45

Note: s is the polymer's side length, H is the polymer's height, t is the surface thickness, Q is the ratio of the surface volume to the polymer volume, $E_{polymer}$ is Young's modulus of the polymer, and $E_{surface}$ is Young's modulus of the surface layer.

Table 9 The ratio of height-to-side length (t/s) with a surface Young's modulus of 10 GPa

s (μm)	H (μm)	$E_{polymer}$ (GPa)	t (μm)	t/s	Q
22	12	0.89	0.007	0.03%	0.19%
20	12	0.88	0.001	0.01%	0.03%
18	12	0.9	0.009	0.05%	0.28%
16	12	1.09	0.09	0.56%	3.00%
14	12	1.36	0.178	1.27%	6.57%
12	12	1.53	0.21	1.75%	8.75%
10	12	1.62	0.2	2.00%	9.67%

Note: s is the polymer's side length, H is the polymer's height, $E_{polymer}$ is Young's modulus of the polymer, t is the surface thickness, and Q is the ratio of the surface volume to the polymer volume.

the side length decreases, Q and $E_{surface}$ tend to increase significantly, which directly leads to the increase of Young's modulus of the polymer. To observe the change in surface thickness under the assumption that $E_{surface}$ is the same, E_1 is set to 5 GPa, and t is solved and listed in Table 9. As the side length decreases, t and Q have a significant increasing trend, which results in an increase in Young's modulus.

Under the assumption of the surface layer properties and thickness of the printed structure, calculated results are consistent with the experimental ones. For the phenomenon of different stiffness of the surface layer, Liu et al. [23,28] pointed out that the linear shrinkage of IP-Dip can reach more than 2%, which is caused by chemical development and drying. Young's modulus with respect to radius is also confirmed by the work of Mozaffari et al. [27]. Based on Gurtin and Murdoch's work [29], they established the strain field describing the surface layer and gave Young's modulus formula for the structure. This shows how the effective or apparent elastic response of the microstructure becomes size-dependent due to surface energy effects. When the radius is small, the effective elastic modulus may be significantly different from its original value. In summary, we hypothesize that the variation of Young's modulus is caused by the surface energy effect in this experiment.

4 Conclusion

In conclusion, micrometric polymeric specimens were printed via two-photon polymerization, and mechanical characterization of the polymer's Young's modulus was calculated. The size effect of IP-Dip significantly affects the magnitude of Young's modulus. The experimental results show that Young's modulus is related to the density of layers and surface energy effect. In the 10–50 μm range that we tested, Young's modulus increased along with the surface-volume ratio. Therefore, due to the surface energy effect, the smaller the structure, the higher the stiffness. The size effect of this material should be considered in nano- or micro-scale printing and high-accuracy design.

Acknowledgment

This work was supported by the 3mE Faculty of Mechanical, Materials, and Maritime Engineering, Department of Precision and Microsystems Engineering of the Delft University of Technology and the China Scholarship Council (CSC). Part of this work was performed at the Dalian University of Technology.

Conflict of Interest

There are no conflicts of interest.

Data Availability Statement

The datasets generated and supporting the findings of this article are obtainable from the corresponding author upon reasonable request.

References

[1] Greer, J. R., and Park, J., 2018, "Additive Manufacturing of Nano- and Microarchitected Materials," Nano Lett., **18**(4), pp. 2187–2188.

[2] Schaedler, T. A., Jacobsen, A. J., Torrents, A., Sorensen, A. E., Lian, J., Greer, J. R., Valdevit, L., and Carter, W. B., 2011, "Ultralight Metallic Microlattices," Science, **334**(6058), pp. 962–965.

[3] Meza, L. R., Zelhofer, A. J., Clarke, N., Mateos, A. J., Kochmann, D. M., and Greer, J. R., 2015, "Resilient 3D Hierarchical Architected Metamaterials," Proc. Natl. Acad. Sci., **112**(37), pp. 11502–11507.

[4] Maggi, A., Allen, J., Desai, T., and Greer, J. R., 2017, "Osteogenic Cell Functionality on 3-Dimensional Nano-Scaffolds With Varying Stiffness," Extrem. Mech. Lett., **13**, pp. 1–9.

[5] Fan, D., Staufer, U., and Accardo, A., 2019, "Engineered 3D Polymer and Hydrogel Microenvironments for Cell Culture Applications," Bioengineering (Basel), **6**(4), p. 113.

[6] Frenzel, T., Kopfler, J., Jung, E., Kadic, M., and Wegener, M., 2019, "Ultrasound Experiments on Acoustical Activity in Chiral Mechanical Metamaterials," Nat. Commun., **10**(1), p. 3384.

[7] Bauer, J., Schroer, A., Schwaiger, R., and Kraft, O., 2016, "Approaching Theoretical Strength in Glassy Carbon Nanolattices," Nat. Mater., **15**(4), pp. 438–443.

[8] Nguyen, A. K., and Narayan, R. J., 2017, "Two-Photon Polymerization for Biological Applications," Mater. Today, **20**(6), pp. 314–322.

[9] Qu, J., Gerber, A., Mayer, F., Kadic, M., and Wegener, M., 2017, "Experiments on Metamaterials With Negative Effective Static Compressibility," Phys. Rev. X, **7**(4), p. 041060.

[10] Kotz, F., Quick, A. S., Risch, P., Martin, T., Hoose, T., Thiel, M., Helmer, D., and Rapp, B. E., 2021, "Two-Photon Polymerization of Nanocomposites for the Fabrication of Transparent Fused Silica Glass Microstructures," Adv. Mater., **33**(9), p. 2006341.

[11] Sharaf, A., Roos, B., Timmerman, R., Kremers, G.-J., Bajramovic, J. J., and Accardo, A., 2022, "Two-Photon Polymerization of 2.5D and 3D Microstructures Fostering a Ramified Resting Phenotype in Primary Microglia," Front. Bioeng. Biotechnol., **10**, p. 926642.

[12] Bažant, Z. P., 2000, "Size Effect," Int. J. Solids Struct., **37**(1–2), pp. 69–80.

Downloaded from http://asmedigitalcollection.asme.org/appliedmechanics/article-pdf/91/1/011002/7036641/jam_91_1_011002.pdf by Bibliotheek Tu Delft user on 18 September 2023

[13] Greer, J. R., and De Hosson, J. T. M., 2011, "Plasticity in Small-Sized Metallic Systems: Intrinsic Versus Extrinsic Size Effect," Prog. Mater. Sci., **56**(6), pp. 654–724.
[14] Albiez, A., and Schwaiger, R., 2019, "Size Effect on the Strength and Deformation Behavior of Glassy Carbon Nanopillars," MRS Adv., **4**(2), pp. 133–138.
[15] Greer, J. R., Oliver, W. C., and Nix, W. D., 2005, "Size Dependence of Mechanical Properties of Gold at the Micron Scale in the Absence of Strain Gradients," Acta Mater., **53**(6), pp. 1821–1830.
[16] Sun, Q., Guo, Q., Yao, X., Xiao, L., Greer, J. R., and Sun, J., 2011, "Size Effects in Strength and Plasticity of Single-Crystalline Titanium Micropillars With Prismatic Slip Orientation," Scr. Mater., **65**(6), pp. 473–476.
[17] Gu, X. W., Loynachan, C. N., Wu, Z., Zhang, Y.-W., Srolovitz, D. J., and Greer, J. R., 2012, "Size-Dependent Deformation of Nanocrystalline Pt Nanopillars," Nano Lett., **12**(12), pp. 6385–6392.
[18] Dottermusch, S., Busko, D., Langenhorst, M., Paetzold, U. W., and Richards, B. S., 2019, "Exposure-Dependent Refractive Index of Nanoscribe IP-Dip Photoresist Layers," Opt. Lett., **44**(1), pp. 29–32.
[19] Liontas, R., and Greer, J. R., 2017, "3D Nano-Architected Metallic Glass: Size Effect Suppresses Catastrophic Failure," Acta Mater., **133**, pp. 393–407.
[20] Arsenault, A. C., Clark, T. J., von Freymann, G., Cademartiri, L., Sapienza, R., Bertolotti, J., Vekris, E., et al., 2006, "From Colour Fingerprinting to the Control of Photoluminescence in Elastic Photonic Crystals," Nat. Mater., **5**(3), pp. 179–184.
[21] Dimitriadis, E. K., Horkay, F., Maresca, J., Kachar, B., and Chadwick, R. S., 2002, "Determination of Elastic Moduli of Thin Layers of Soft Material Using the Atomic Force Microscope," Biophys. J., **82**(5), pp. 2798–2810.
[22] Lemma, E. D., Rizzi, F., Dattoma, T., Spagnolo, B., Sileo, L., Qualtieri, A., De Vittorio, M., and Pisanello, F., 2016, "Mechanical Properties Tunability of Three-Dimensional Polymeric Structures in Two-Photon Lithography," IEEE Trans. Nanotechnol., **16**(1), pp. 23–31.
[23] Liu, Y., Campbell, J., Stein, O., Jiang, L., Hund, J., and Lu, Y., 2018, "Deformation Behavior of Foam Laser Targets Fabricated by Two-Photon Polymerization," Nanomaterials, **8**(7), p. 498.
[24] Montemayor, L. C., and Greer, J. R., 2015, "Mechanical Response of Hollow Metallic Nanolattices: Combining Structural and Material Size Effects," ASME J. Appl. Mech., **82**(7), p. 071012.
[25] Sharaf, A., Frimat, J. P., Kremers, G. J., and Accardo, A., 2023, "Suppression of Auto-Fluorescence From High-Resolution 3D Polymeric Architectures Fabricated Via Two-Photon Polymerization for Cell Biology Applications," Micro Nano Eng., **19**, p. 100188.
[26] van Altena, P. F. J., and Accardo, A., 2023, "Micro 3D Printing Elastomeric IP-PDMS Using Two-Photon Polymerisation: A Comparative Analysis of Mechanical and Feature Resolution Properties," Polymers, **15**(8), p. 1816.
[27] Mozaffari, K., Yang, S., and Sharma, P., 2020, "Surface Energy and Nanoscale Mechanics," *Handbook of Materials Modeling: Applications: Current and Emerging Materials*, Springer International, Cham, pp. 1949–1974.
[28] Liu, Y., Stein, O., Campbell, J. H., Jiang, L., Petta, N., and Lu, Y., 2017, "Three-Dimensional Printing and Deformation Behavior of Low-Density Target Structures by Two-Photon Polymerization," Nanoeng.: Fabr., Prop., Opt. Devices XIV, **10354**, p. 103541U.
[29] Gurtin, M. E., and Ian Murdoch, A., 1975, "A Continuum Theory of Elastic Material Surfaces," Arch. Rational Mech. Anal., **57**(4), pp. 291–323.

Downloaded from http://asmedigitalcollection.asme.org/appliedmechanics/article-pdf/91/1/011002/7036641/jam_91_1_011002.pdf by Bibliotheek Tu Delft user on 18 September 2023